Micromagnetic understanding of the skyrmion Hall angle current dependence in perpendicularly magnetized ferromagnets

Riccardo Tomasello,[1] Anna Giordano,[2] Stefano Chiappini,[3] Roberto Zivieri,[2] Giulio Siracusano,[4] Vito Puliafito,[5] Israa Medlej,[2] Aurelio La Corte,[4] Bruno Azzerboni,[5] Mario Carpentieri,[6] Zhongming Zeng,[7] and Giovanni Finocchio[2,3]

[1]*Institute of Applied and Computational Mathematics, FORTH, GR-70013 Heraklion-Crete, Greece*

[2]*Department of Mathematical and Computer Sciences, Physical Sciences and Earth Sciences, University of Messina, I-98166 Messina, Italy*

[3]*Istituto Nazionale di Geofisica e Vulcanologia, Via di Vigna Murata 605, I-00143 Roma, Italy*

[4]*Department of Electric, Electronic, and Computer Engineering, University of Catania, I-95125 Catania, Italy*

[5]*Department of Engineering, University of Messina, I-98166 Messina, Italy*

[6]*Department of Electrical and Information Engineering, Politecnico di Bari, I-70125 Bari, Italy*

[7]*Key Laboratory of Nanodevices and Applications, Suzhou Institute of Nano-tech and Nano-bionics, Chinese Academy of Sciences, Ruoshui Road 398, Suzhou 215123, People's Republic of China*

(Received 31 July 2018; revised manuscript received 28 November 2018; published 17 December 2018)

The understanding of the dynamical properties of skyrmions is a fundamental aspect for the realization of a competitive skyrmion based technology beyond complementary metal-oxide semiconductors. Most of the theoretical approaches are based on the approximation of a rigid skyrmion. However, thermal fluctuations can drive a continuous change of the skyrmion size via the excitation of thermal modes. Here, by taking advantage of the Hilbert-Huang transform, we demonstrate that at least two thermal modes can be excited which are nonstationary in time. In addition, one limit of the rigid skyrmion approximation is that this hypothesis does not allow for correctly describing the recent experimental evidence of skyrmion Hall angle dependence on the amplitude of the driving force, which is proportional to the injected current. In this paper, we show that, in an ideal sample, the combined effect of fieldlike and dampinglike torques on a breathing skyrmion can indeed give rise to such a current dependent skyrmion Hall angle. While here we design and control the breathing mode of the skyrmion, our results can be linked to the experiments by considering that the thermal fluctuations and/or disorder can excite the breathing mode. We also develop a generalized Thiele equation and propose an experiment to validate our findings.

DOI: 10.1103/PhysRevB.98.224418

I. INTRODUCTION

Magnetic skyrmions are localized swirling perturbations of the uniform magnetization texture [1–3] which can be stabilized by a sufficiently large Dzyaloshinskii-Moriya interaction (DMI) [4,5]. The DMI arises in systems with broken inversion symmetry, such as noncentrosymmetric bulk magnetic compounds (bulk DMI) [6–8], multilayered heterostructures where a thin ferromagnet is in contact with a nonmagnetic heavy metal with strong spin-orbit interaction [interfacial DMI (IDMI)] [9–14], or Heusler materials with tetragonal inverse structure (DMI in D_{2d} structures) [15–17]. According to the kind of DMI, different types of skyrmions can be stabilized: Bloch skyrmions (vortexlike configuration) for bulk DMI materials, Néel skyrmions (hedgehog configuration) in IDMI systems, and antiskyrmions in D_{2d} structures.

Skyrmions can be very small (diameters of the order of nanometers), energetically stable, and topologically protected [2,3] because they are characterized by an integer winding number S [18]. Owing to these features, together with the fact that they can be manipulated (nucleated, moved, and annihilated) by electrical currents [9,11,14,19], skyrmions are becoming attractive candidates to be used in low-power microelectronic applications, as building blocks of storage and programmable logic, as well as in alternative computational paradigms, such as probabilistic computing and skyrmion fabrics [20].

Recently, intense research efforts have led to the identification of multilayer heterostructures where Néel skyrmions are stable at room temperature and can be shifted by spin-orbit torque (SOT) [12–14]. To study the skyrmion stability, we have previously introduced a nonlinear ansatz [21] that can be used, together with proper scaling relations of the magnetic parameters, to analyze skyrmion stability and average size (diameter) as a function of the external field and temperature. In addition, it has been also shown that the thermal effects induce internal distortions of the skyrmion, which then loses its circular symmetry [21], expansion and shrinking of the skyrmion core (thermal breathing mode), and a thermal drift [22] (gyrotropic motion). The first result of this paper concerns the identification of the nonstationary origin of the skyrmion modes excited by thermal fluctuations.

Skyrmion motion can be driven by the spin-transfer torque (STT) [9,10,23] from an in-plane current flowing in the ferromagnets [24], or, more efficiently [9,10], by the SOT due to the spin-Hall effect (SHE) [25] and to the inverse spin-Galvanic effect [26], originating from a current flowing via a heavy metal with large spin-orbit coupling in contact with a ferromagnet. The skyrmion shifting is characterized by an in-plane angle with respect to the direction of the applied current, i.e., the skyrmion Hall angle (SHA) [27–29].

The control of the SHA is crucial for racetrack memory applications where skyrmions, coding the information, would be inevitably driven towards the sample edges where they could either bounce back or be annihilated. This aspect also limits the maximum applicable current and hence the maximum velocity achievable for the skyrmion. One strategy to overcome this issue is to suppress the SHA by balancing the Magnus force in two coupled skyrmions with opposite topological charge, resulting in zero net topological charge, in ferrimagnets [30], synthetic antiferromagnets [31,32], or antiferromagnets [33].

In an ideal ferromagnet/heavy metal bilayer, micromagnetic simulations and the theoretical approaches based on the Thiele formalism including the dampinglike torque (DLT) and the rigid skyrmion approximation predict a constant SHA that is independent of the value of the applied current [10,27–29]. In particular, with our set of parameters [10], such a motion is characterized by a current-independent SHA ϕ_{SkH} equal to $\sim -90^{\circ}$ with respect to the direction of a positive current along a positive x direction (the SHA can be computed by the skyrmion velocity components as $\arctan(v_y/v_x)$). In other words, the skyrmion moves mainly along the negative y direction with a small negative x component of the velocity [10], and vice versa for negative currents.

In contrast, recent experimental observations have shown a current dependence of the SHA. Jiang *et al.* [27] attributed such dependence to the presence of random pinning potentials in their materials. Basically, at low currents in the so-called creep regime, the skyrmion motion is strongly affected by pinning from defects and its SHA is current dependent, whereas, at high currents, the skyrmion is characterized by a steady-flow regime where its SHA is independent of the current. Differently, Litzius *et al.* [28] claimed that the current dependence of the SHA results from the combination of the SHE fieldlike torque (FLT) [34] and the internal deformations of the skyrmion. In order to add our contribution to this debate, we performed micromagnetic simulations where FLT and DLT are simultaneously applied to a breathing skyrmion. Our results show the qualitative picture that fundamentally explains the current dependent SHA. The paper is organized as follows. Section II presents the details of the micromagnetic framework. Section III shows the results of this paper, with particular focus on the identification of the thermal breathing modes and on the control of the skyrmion Hall angle. Section IV is dedicated to the discussion of our results, where we also propose a generalized Thiele equation to qualitatively confirm our achievements as well as an experiment to quantify the effect of the FLT. The conclusions are reported in Sec. V.

II. MICROMAGNETIC MODEL

We analyze a square sample where a thin ferromagnetic layer is in contact with a platinum underlayer in order to obtain the IDMI and SHE. The micromagnetic study is performed by means of state-of-the-art processing tools and home-made micromagnetic solver GPMagnet [35,36] which numerically integrates the Landau-Lifshitz-Gilbert-Slonczewski equation by applying the time solver scheme Adams-Bashforth, where the SHE-FLT and SHE-DLT are taken into account:

$$\begin{aligned}\frac{d\mathbf{m}}{d\tau} = &-(\mathbf{m}\times\mathbf{h}_{\mathbf{eff}}) - \alpha\left(\mathbf{m}\times\frac{d\mathbf{m}}{d\tau}\right)\\ &- d_j\{\mathbf{m}\times[\mathbf{m}\times(\hat{z}\times\mathbf{j}_{\mathbf{HM}})]\}\\ &- \nu d_j[\mathbf{m}\times(\hat{z}\times\mathbf{j}_{\mathbf{HM}})] \qquad (1)\end{aligned}$$

where $\mathbf{m} = \mathbf{M}/M_s$ is the normalized magnetization of the ferromagnet and $\tau = \gamma_0 M_s t$ is the dimensionless time, with γ_0 being the gyromagnetic ratio and M_s the saturation magnetization. $\mathbf{h}_{\mathbf{eff}}$ is the normalized effective field, which includes the exchange, IDMI, magnetostatic, anisotropy, and external fields. α is the Gilbert damping. $d_j = \frac{g\mu_B\theta_{\mathrm{SH}}}{2\gamma_0 e M_S^2 t_{\mathrm{FM}}}$ where g is the Landé factor, μ_B is the Bohr magneton, θ_{SH} is the spin-Hall angle, e is the electron charge, and t_{FM} is the thickness of the ferromagnetic layer. $\hat{z}$ is the unit vector along the out-of-plane direction, and $\mathbf{j}_{\mathbf{HM}}$ is the electrical current density flowing into the Pt heavy metal which gives rise to the SHE. ν is a coefficient linking the magnitude of the FLT to the one of the DLT [34].

The lateral dimension of the square sample under investigation is 1.6 μm, while the ferromagnet thickness is $t_{\mathrm{FM}} =$ 1 nm. The discretization cell used in the simulations is $2.0 \times 2.0 \times 1.0\,\mathrm{nm}^3$. We introduce a Cartesian coordinate system with the x and y axes lying in the plane of the sample, whereas the z axis is oriented along the out-of-plane direction. We consider typical parameters for CoFeB/Pt bilayers [10]: $M_S =$ 1000 kA/m, exchange constant $A = 20\,\mathrm{pJ/m}$, perpendicular anisotropy constant $k_u = 0.80\,\mathrm{MJ/m}^3$, $D = 2.0\,\mathrm{mJ/m}^2$, $\alpha =$ 0.03, and $\theta_{\mathrm{SH}} = 0.1$. The current j_{HM} flows in the x direction, thus the spin current inside the heavy metal is polarized along the y direction. We apply an out-of-plane external field $H_z =$ 25 mT in all the simulations to have a metastable skyrmion [21] and to reduce the transient breathing mode. The SHE-FLT has the direction of the spin polarization (y axis). In order to deeply understand the role of the SHE-FLT and the physics underlying the SHA current dependence, we consider, in the first part of the paper, a constant FLT $|\nu d_j j_{\mathrm{HM}} M_s| = |H_{\mathrm{FLT}}| = 50\,\mathrm{mT}$, while, in the second part, we fix the DLT and we change the FLT.

For stochastic simulations, the thermal fluctuations are added to the deterministic effective magnetic field as a random term in each computational $\mathbf{h}_{\mathrm{th}} = (\chi/M_S)\sqrt{2(\alpha K_B T/\mu_0\gamma_0\Delta V\, M_s\, \Delta t)}$, with K_B being the Boltzmann constant, ΔV the volume of the computational cubic cell, Δt the simulation time step, T the temperature of the sample, and χ a three-dimensional white Gaussian noise with zero mean and unit variance [37,38]. The noise is assumed to be uncorrelated for each computational cell.

III. RESULTS

A. Nonstationary behavior of thermal breathing modes

Thermal fluctuations can drive both a drift of the skyrmion, which has been also experimentally observed [39], and thermal modes, the presence of which has been only shown by micromagnetic simulations [21] up to date. In this paper, we have developed a technique that identifies such thermal modes from the time domain evolution of the skyrmion area as computed by micromagnetic simulations. For this purpose,

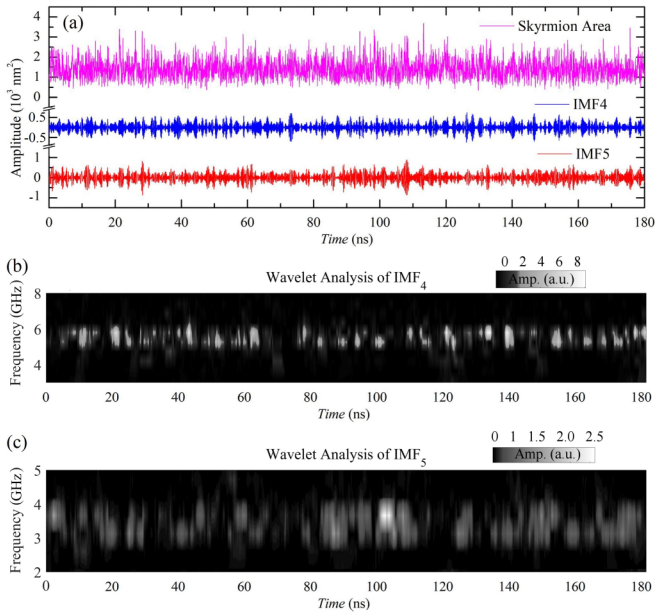

FIG. 1. (a) Time evolution of the skyrmion area (magenta curve) when $H_z = 25$ mT and $T = 300$ K and corresponding most significant IMFs (blue and red curves), as obtained by HHT analysis. (b, c) Wavelet results of IMF4 and IMF5, respectively, where the color scale indicates the amplitude of the signal.

we combine the Hilbert-Huang transform [40–42] (HHT; see Supplemental Material [43], note 1) and the wavelet transform [44,45]. The former aims at decomposing the signal into independent oscillatory components, also known as intrinsic mode functions (IMFs), in order to identify the time domain traces of the thermal modes. The latter studies the nonstationary behavior of those modes. We consider the data computed in our previous work [21]. In particular, the magenta curve in Fig. 1(a) represents an example of the time trace of the skyrmion area at $T = 300$ K and $H_z = 25$ mT (similar results are obtained for each combination of temperature and external field, where temperature ranges from 50 to 300 K with steps of 50 K and the field is 0, 25, and 50 mT; see Supplemental Material [43], movie 1). The skyrmion area is considered as the area of the region where the magnetization of the skyrmion core (negative z component) is smaller than zero [21].

The HHT based computations show the existence of two IMFs that are correlated to the time domain trace of the skyrmion area. In Fig. 1(a), those two IMFs (IMF4 in blue and IMF5 in red) are represented as a function of time. Although the HHT is a powerful tool for analyzing complex datasets, many irrelevant IMFs may appear in the decomposition. A statistical significance of IMFs [46,47] uses a statistically based threshold to discriminate between relevant and irrelevant IMFs. However, it has been shown how, for very noisy signals, both of these methods perform poorly [48]. Here, the criterion used for the classification of the IMFs in terms of significance is based on the evaluation of the normalized cross correlations (CC) at a lag of zero [49,50] between the signal of the skyrmion area, x, and each IMF component (a complete description of the method is provided in Supplemental Material [43], note 1). In detail, the HHT decomposes the signal, $x(t)$, into a finite number N of different IMFs $y_i = y_i(t)$ (for $i = 1, \ldots, N$), such that $x \cong \sum_{i=1}^{N} y_i$. For the ith IMF, the cross correlation with x, $\hat{R}_{x,y_i}$, can be defined as [50]

$$\hat{R}_{x,y_i}[m] = \begin{cases} \sum_{n=0}^{L-m-1} x[n+m]y_i^*[n] \; m > 0 \\ \hat{R}^*_{y_i,x}[-m] \; m < 0 \end{cases} \quad (2)$$

where $y_i{}^*$ is the complex conjugate of y_i. The value $\mathrm{CC}_i = \frac{\hat{R}_{x,y_i}[0]}{\|x\| \cdot \|y_i\|}$ represents the normalized cross correlation at a lag of zero ($-1 \leqslant \mathrm{CC}_i \leqslant 1$). The correlation is computed according to Eq. (2) and the results of the computation for all the IMFs are reported in Table I for the case under investigation ($H_z = 25$ mT, $T = 300$ K). The relevance of IMFs is established by evaluating the corresponding CC values and peak frequency values (f_{peak}). For example, for the case investigated in Fig. 1, the most relevant IMFs are IMF4 and IMF5, although there are other modes with high CC, but with relatively low-frequency fluctuations (such as the sub-gigahertz modes indicated with IMF11 and IMF15), which are far from the frequencies obtained by deterministic micromagnetic simulations (see below).

TABLE I. Results of HHT for the skyrmion area signal as investigated in Fig. 1. Cross-correlation (CC) of corresponding IMFs and peak frequency values (f_{peak}), respectively.

IMF number	|CC|	f_{peak} (GHz)
IMF1	0.029	58.86
IMF2	0.020	27.56
IMF3	0.046	7.41
IMF4	**0.128**	**5.33**
IMF5	**0.154**	**3.54**
IMF6	0.117	2.04
IMF7	0.101	1.07
IMF8	0.077	0.115
IMF9	0.041	0.142
IMF10	0.0911	0.121
IMF11	0.171	0.079
IMF12	0.083	0.031
IMF13	0.061	0.021
IMF14	0.039	0.010
IMF15	0.331	0.005

In addition to the fast Fourier transform that shows a main frequency component of 5.45 GHz for IMF4 and of 3.54 GHz for IMF5, we perform a wavelet analysis (see Supplemental Material [43], note 2). Figures 1(b) and 1(c) show the wavelet scalogram [51] that clearly brings the conclusion of the nonstationary feature of those two thermal modes.

To show that those excitations are linked to the skyrmion breathing, we carried out deterministic micromagnetic simulations by using the value of the physical parameters as calculated by scaling relations [21,52] (see Supplemental Material [43], note 3 and movie 2). We observe that the FMR frequency of the skyrmion breathing mode lies inside the frequency range identified by the most significant IMFs' frequencies. For instance, for the case shown in Fig. 1 ($H_z = 25$ mT, $T = 300$ K), the FMR frequency is 5.0 GHz and it is comprised between 3.54 GHz (IMF5) and 5.45 GHz (IMF4).

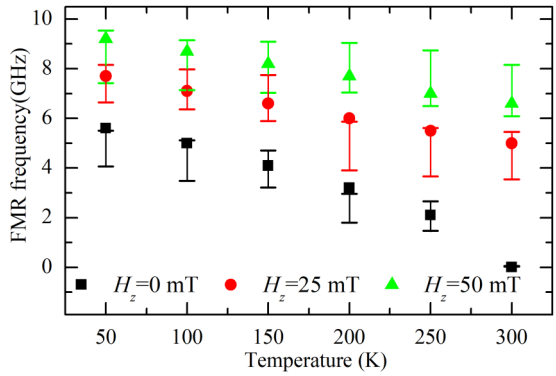

FIG. 2. FMR frequency as a function of temperature and external field, where the symbols represent the results as obtained by micromagnetic simulations by using scaling relations of the physical parameters, while the two dashed indicate the frequency of the two most significant IMFs.

This achievement, that is the first main result of this paper, is robust for each field-temperature combination, as can be observed in Fig. 2, which displays the FMR frequencies (symbols in the figure) and the thermal modes frequencies (dashes in the figure) as a function of temperature (50–300 K) at three different fields (0, 25, and 50 mT).

B. Study of the skyrmion Hall angle

The computations discussed in the previous paragraph show that thermal fluctuations excite nonstationary breathing modes. It is also well known that disorder physical parameters can give rise to a continuous change of the skyrmion size [53], hence we conclude that the nonstationary breathing mode should have a role in the explanation of the SHA current dependence found in the experiments [27,28]. In addition, it has been already shown that the combination of an in-plane field and a breathing mode induces a Bloch skyrmion shift [54]. With this in mind, we have designed a numerical experiment to investigate the dynamical properties of a breathing Néel skyrmion driven by the FLT and DLT. In order to excite the skyrmion breathing mode by means of an ac perpendicular spin-polarized current [see sketch in Fig. 3(a)] to resemble the effect of thermal fluctuations and/or disordered physical parameters, we add to Eq. (1) the following STT term [55]:

$$-\frac{g\mu_B j_P}{\gamma_0 e M_S^2 t_{\mathrm{FM}}}\varepsilon_{\mathrm{MTJ}}(\mathbf{m},\mathbf{m_p})[\mathbf{m}\times(\mathbf{m}\times\mathbf{m_p})] \qquad (3)$$

where $j_P = J_{\mathrm{AMP}}\sin(2\pi f t)$ is the ac current density, with J_{AMP} and f being its amplitude and frequency, respectively. $\varepsilon_{\mathrm{MTJ}}(\mathbf{m},\mathbf{m_p}) = \frac{2\eta}{[1+\eta^2(\mathbf{m}\cdot\mathbf{m_p})]}$ is the polarization function [56,57], where $\eta = 0.66$ is the spin-polarization factor and $\mathbf{m_p}$ is the magnetization of the polarizer, which is considered fixed along the out-of-plane direction, thus generating a perpendicularly polarized spin current.

For this paper, we consider the same parameters already used in Ref. [10] for a direct comparison. The features of the skyrmion dynamics are described in terms of SHA and x and y components of the skyrmion velocity. To this aim, we introduce a Cartesian coordinate reference system, as indicated in the inset of Fig. 5(a), where also the SHA is represented.

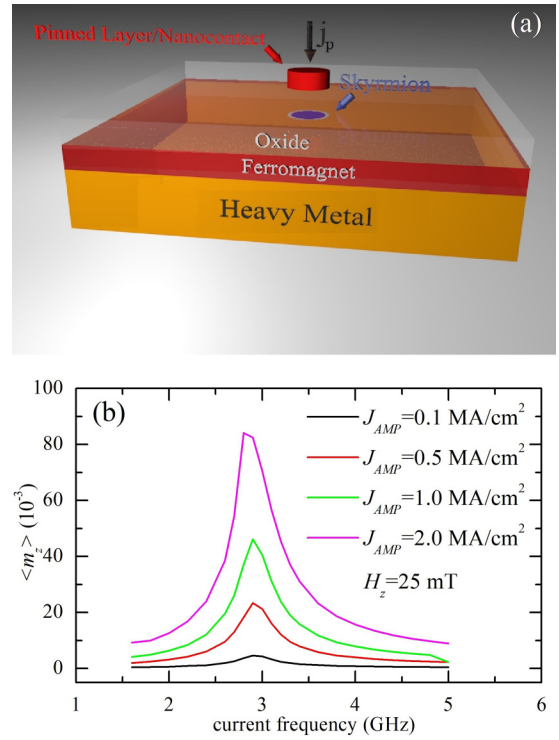

FIG. 3. (a) Sketch of the device under investigation to study the FMR response of the skyrmion, where the ac perpendicular current is locally injected via a nanocontact. (b) FMR frequency response driven by the ac perpendicular current when $H_z = 25$ mT and $T = 0$ K, for different values of J_{AMP} as indicated in the legend.

1. Characterization of the breathing modes

The skyrmion dynamics in the presence of a persistent breathing mode are studied at $T = 0$ K and $H_z = 25$ mT, in order to obtain some simple and fundamental achievements. Figure 3(b) shows the FMR response of the skyrmion, where the peak-to-peak amplitude of $\langle m_z\rangle$ is plotted as a function of the ac current frequency f. For the range of J_{AMP} plotted, the response is linear with a FMR frequency equal to 2.9 GHz, in qualitative agreement with previous studies [55,58]. However, the presence of H_z introduces an upper threshold for the applied current (in our case 2.0 MA/cm^2) over which the skyrmion is annihilated for frequencies near the FMR one. This occurs because, during a half period of the current, H_z favors the skyrmion shrinking, which becomes critical over a certain value of the current amplitude.

For the current-driven dynamics of the skyrmion, to avoid skyrmion annihilation, we consider ac currents with frequencies larger than the FMR one, i.e., $f \gtrsim 3.0$ GHz, and we will focus on two cases: the small breathing mode, where the perpendicular current amplitude J_{AMP} is 2 MA/cm^2, and the large breathing mode, with J_{AMP} equal to 6 MA/cm^2 (note that far from the resonant frequency the skyrmion does not annihilate at this current density).

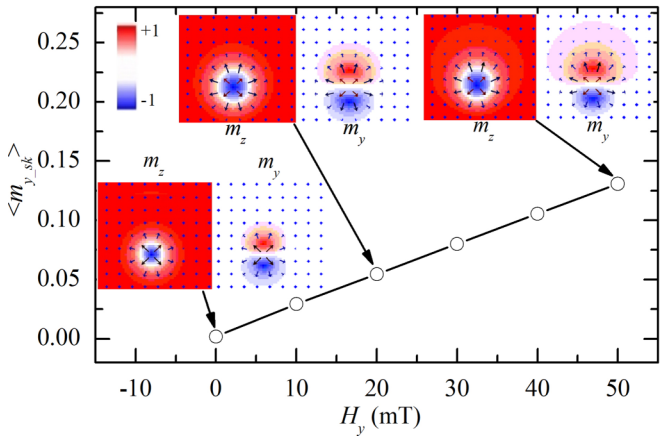

FIG. 4. Average y component of the magnetization of the skyrmion as a function of the in-plane field. Inset: Spatial distribution of the magnetization displaying the skyrmion for $H_{\mathrm{FLT}} = 0$, 20, and 50 mT. The left panel represents the z component of the magnetization, while the right panel represents the y component. The same color scale for both components is also indicated.

2. *Effect of the fieldlike torque*

When considering a rigid skyrmion, its motion driven by the DLT is not affected by the FLT (see Supplemental Material [43], movie 3). In particular, the role of the FLT is to elongate the skyrmion along the direction of the in-plane field [54,59] leading to a noncircular skyrmion, without modifying the skyrmion velocity and SHA, but only the maximum applicable current. This result is in agreement with previous works on Bloch skyrmions [59]. Figure 4 displays such a deformation along the field direction, where the main panel shows the spatial-averaged y component of the skyrmion magnetization $\langle m_{y\_\mathrm{sk}} \rangle$ as a function of the in-plane field. As expected, $\langle m_{y\_\mathrm{sk}} \rangle$ is almost zero at zero field because the skyrmion is symmetric and circular, while it increases linearly with the field. This result is confirmed by the spatial distribution of the skyrmion magnetization (insets in Fig. 4), where we can observe how the skyrmion becomes noncircular as the field increases.

3. *Effect of the breathing mode*

Now, we consider a breathing skyrmion. Its motion driven by the DLT in the term of SHA does not differ from the rigid one, because the periodic change of the skyrmion radios has a null effect on average (not shown, see Supplemental Material [43], movie 3). In contrast, the FLT gives rise to a skyrmion shift along the x direction (same direction of the electrical current) because the in-plane field breaks the skyrmion symmetry, as already predicted for Bloch skyrmions [54]. Therefore, the breathing skyrmion undergoes two antagonistic effects: from one side, the DLT moves it mainly along the y direction; from the other side, the FLT moves it along the x direction. This aspect will allow us to control the SHA, as it will be shown in the next paragraph.

4. *Dynamics driven by SHE-DLT and SHE-FLT in the presence of the breathing mode*

In this paragraph, we show the results obtained when SHE-DLT and SHE-FLT act simultaneously on a breathing skyrmion. We fix the current j_{HM} flowing into the heavy metal to $-5\,\mathrm{MA/cm^2}$ and we use two values of FLT that correspond to $H_{\mathrm{FLT}} = \pm 50\,\mathrm{mT}$. Figures 5(a)–5(c) show the results for small breathing. Although there is a slight variation of ϕ_{SkH}, v_x, and v_y, this can be considered negligible. In contrast, when the breathing becomes larger [Figs. 5(d)–5(f)], we observe that the x component of the velocity is negative for all the frequencies for negative values of the in-plane field. In other words, as expected, the FLT affects mainly v_x, promoting a skyrmion displacement along the positive (negative)

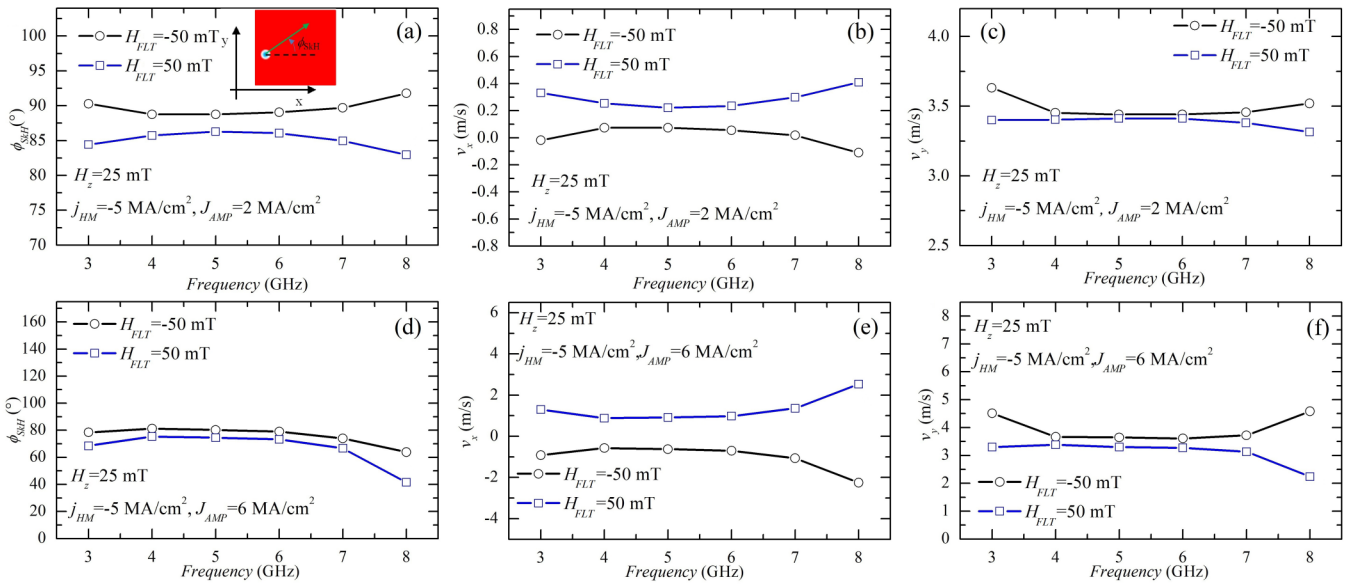

FIG. 5. Skyrmion dynamics (ϕ_{SkH}, v_x, and v_y) as a function of the breathing mode frequency for $H_{\mathrm{FLT}} = 50\,\mathrm{mT}$ (blue curve with squares) and $-50\,\mathrm{mT}$ (black curve with circles), when $H_z = 25\,\mathrm{mT}$, $j_{\mathrm{HM}} = -5\,\mathrm{MA/cm^2}$, and (a–c) $J_{\mathrm{AMP}} = 2\,\mathrm{MA/cm^2}$ and (d–f) $J_{\mathrm{AMP}} = 6\,\mathrm{MA/cm^2}$. In (a), ϕ_{SkH} is calculated with respect to the positive x axis. In (d), ϕ_{SkH} is calculated with respect to the negative x axis when $H_{\mathrm{FLT}} = -50\,\mathrm{mT}$.

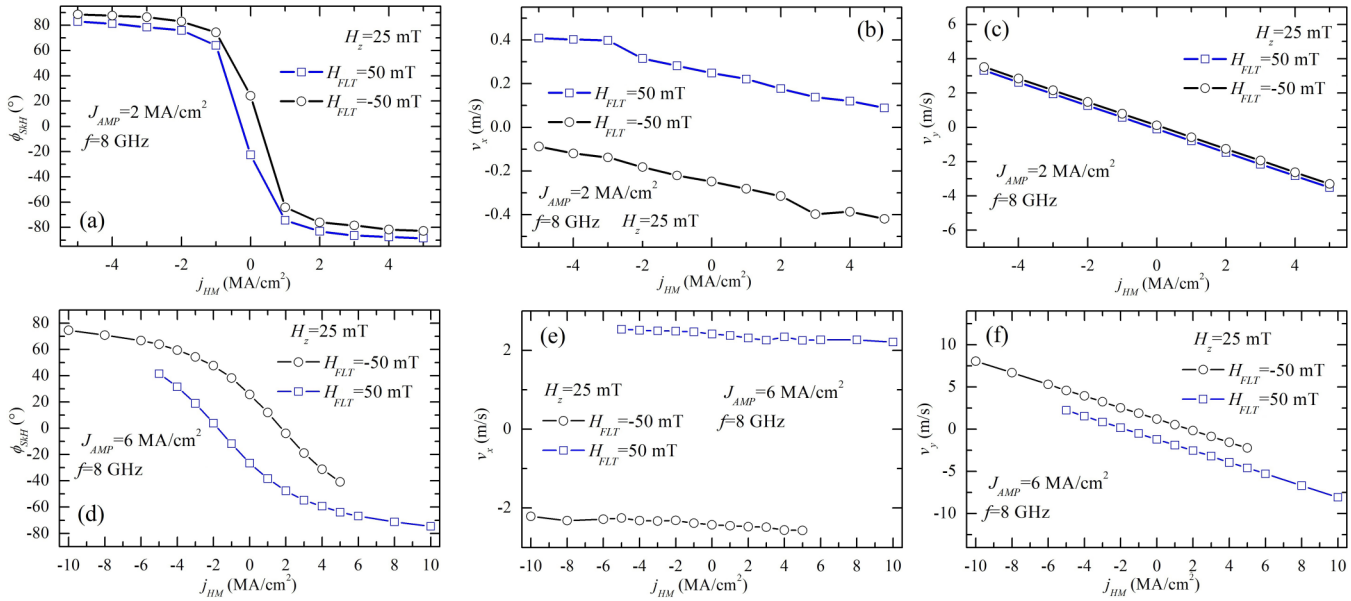

FIG. 6. Skyrmion dynamics as a function of SHE-DLT, where ϕ_{SkH}, v_x, and v_y are represented with regards to the in-plane current j_{HM}, for $H_{\mathrm{FLT}} = 50\,\mathrm{mT}$ (blue curve with squares) and $-50\,\mathrm{mT}$ (black curve with circles), when $H_z = 25\,\mathrm{mT}$, $f = 8\,\mathrm{GHz}$, and (a–c) $J_{\mathrm{AMP}} = 2\,\mathrm{MA/cm^2}$ and (d–f) $J_{\mathrm{AMP}} = 6\,\mathrm{MA/cm^2}$. In (a) and (d), ϕ_{SkH} is calculated with respect to the negative x axis when $H_{\mathrm{FLT}} = -50\,\mathrm{mT}$.

x direction for positive (negative) values of the field, while the DLT influences the y component of the velocity. It is important to notice that, in Fig. 1(d), for $H_{\mathrm{FLT}} = -50\,\mathrm{mT}$, ϕ_{SkH} is computed with respect to the negative x axis. In addition, the small change of the ϕ_{SkH} as a function of frequency is still negligible. In the rest of the paper, we will focus on a frequency of 8 GHz to speed up the computations, however simulations performed at different frequencies do not exhibit any qualitative difference.

We now study the skyrmion dynamics by changing the value of j_{HM} (SHE-DLT), at a fixed $H_{\mathrm{FLT}} = \pm 50\,\mathrm{mT}$ (SHE-FLT). It is interesting to observe in Fig. 6 that also for $j_{\mathrm{HM}} = 0\,\mathrm{MA/cm^2}$ we obtain the skyrmion motion, but with a major component along the positive (negative) x direction if the field is positive (negative). In other words, the combination of only FLT and breathing mode promotes the skyrmion shift in the same direction of the electrical current. When we increase the magnitude of j_{HM}, the DLT, which drives the skyrmion mainly in the direction perpendicular to the electrical current, leads ϕ_{SkH} to be almost 90° from very low currents in the case of small breathing [$j_{\mathrm{HM}} > 1\,\mathrm{MA/cm^2}$ in Fig. 6(a)]. A smaller frequency of the breathing mode will shift the curve in Fig. 6(a) to lower current values.

The x component of the velocity [Fig. 6(b)] slightly changes with current. This is due to the fact that it is of the same order as the one induced by the DLT. In particular, a positive (negative) current introduces a v_x of the same sign as the one due to the FLT for negative (positive) fields, hence the magnitude of v_x increases. The y component of the velocity is not affected by the FLT [Fig. 6(c)] because the blue and black curves coincide.

If the breathing is larger, ϕ_{SkH} slowly increases with current and starts to saturate to 76° for currents larger than $5\,\mathrm{MA/cm^2}$ [Fig. 6(d)]. This behavior is in qualitative agreement with the experimental evidences [27,28] [see, for instance, Fig. 3(c) of Ref. [27]]. In addition, it is more evident that the combination of FLT and breathing mode introduces a smaller y component of the velocity. In fact, at zero j_{HM}, ϕ_{SkH} is about 30°. The larger breathing mode enhances also the effect of the FLT, i.e., v_x is almost constant with current, meaning that the x-axis skyrmion motion is dominated by the FLT [Fig. 6(e)]. Owing to the smaller v_y induced by the FLT, also the total v_y is affected; in fact the two curves are no longer overlapped [Fig. 6(f)]. In all the cases, we observe a symmetric skyrmion dynamics with respect to the sign of the current.

Finally, we study the skyrmion dynamics by changing the value of H_{FLT} (SHE-FLT), when $j_{\mathrm{HM}} = \pm 5\,\mathrm{MA/cm^2}$. When the breathing is small [Figs. 7(a)–7(c)], the FLT slightly affects only the x component of the velocity, while ϕ_{SkH} and v_y keep constant with fields. In particular, the magnitude of v_x increases with positive (negative) fields when the current is negative (positive), as explained above for Fig. 6(b).

When the breathing mode becomes larger [Figs. 7(d)–7(f)], the FLT has a dominant effect. The magnitude of ϕ_{SkH} increases (decreases) for negative (positive) values of H_{FLT}, while v_x is almost independent of the DLT [Fig. 7(e)]. In addition, Fig. 7(f) shows that the y component of the velocity, which is typically due to the DLT, is also affected by the FLT, that leads to a larger magnitude of v_y when the FLT has the same direction as the DLT (H_{FLT} has the same sing as j_{HM}). Again, these achievements demonstrate that an appropriate combination of SHE-DLT, SHE-FLT, and breathing mode allows one to control the direction of the skyrmion motion.

IV. DISCUSSION

These results clearly show that the key aspect which gives rise to the experimental current dependence of the SHA [27,28] is the combination of the breathing mode (due to thermal fluctuations and/or internal defects) and a sufficiently

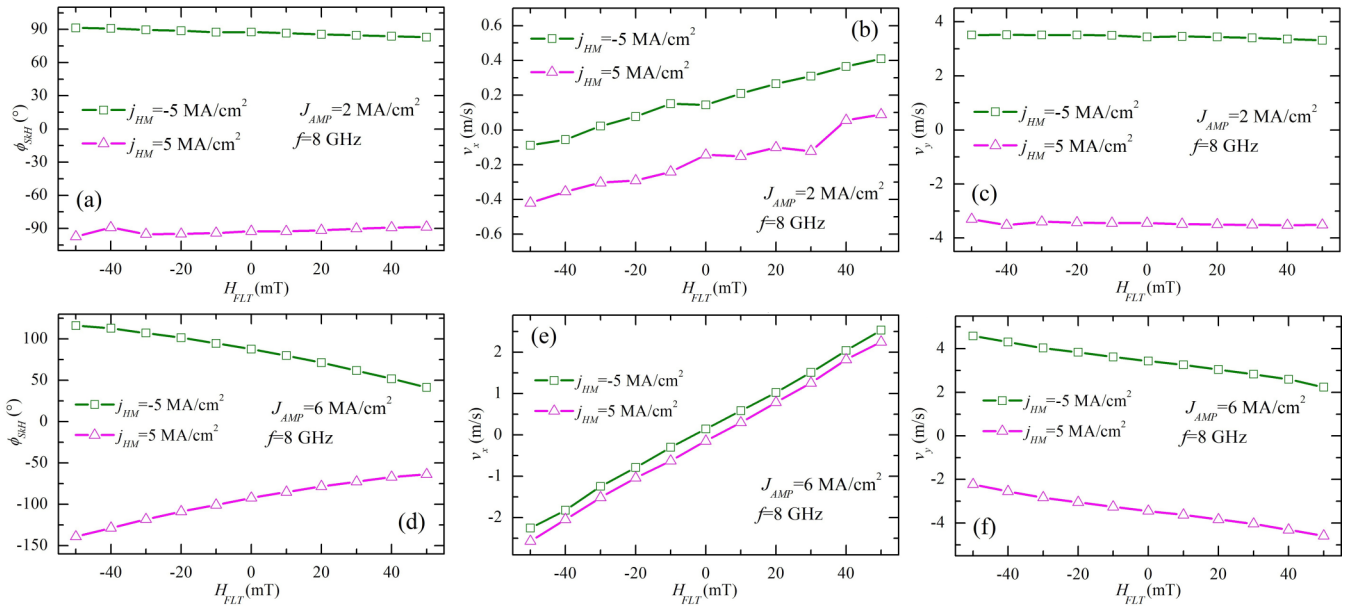

FIG. 7. Skyrmion dynamics as a function of the SHE-FLT, where ϕ_{SkH}, v_x, and v_y are plotted with regards to the in-plane field H_{FLT}, for $j_{\mathrm{HM}} = 5\,\mathrm{MA/cm^2}$ (olive curve with squares) and $-5\,\mathrm{MA/cm^2}$ (magenta curve with triangles), when $H_z = 25\,\mathrm{mT}$, $f = 8\,\mathrm{GHz}$, and (a–c) $J_{\mathrm{AMP}} = 2\,\mathrm{MA/cm^2}$ and (d–f) $J_{\mathrm{AMP}} = 6\,\mathrm{MA/cm^2}$. In (a) and (d), ϕ_{SkH} is calculated with respect to the positive x axis.

large SHE-FLT. For the sake of clarity, Table II summarizes the properties of the skyrmion motion by combining all of those ingredients. As it can be observed, the slope of the region where ϕ_{SkH} depends on current is smaller (larger current region) as the amplitude of the breathing mode increases. In detail, if the breathing is small (results for $J_{\mathrm{AMP}} = 2\,\mathrm{MA/cm^2}$), the SHA saturates for $|j_{\mathrm{HM}}| > 2\,\mathrm{MA/cm^2}$. When the breathing is large (results for $J_{\mathrm{AMP}} = 6\,\mathrm{MA/cm^2}$), the SHA is still not completely saturated up to $|j_{\mathrm{HM}}| > 10\,\mathrm{MA/cm^2}$. In other words, the larger the breathing mode the larger its effect on the skyrmion dynamics and therefore on the range of current dependence of the SHA. If we want to link this result to an experiment, it means that a more pronounced breathing, i.e., larger disorder and/or temperature, will lead to a larger region where the ϕ_{SkH} depends on current. To confirm those conclusions and resolve the debate discussed in the Introduction, it would be sufficient to characterize ϕ_{SkH} as a function of an in-plane field for different currents. When the in-plane field is parallel to the fieldlike torque, ϕ_{SkH} current dependence should be more evident [smaller slope, Fig. 6(d) for example], as compared to the case when the in-plane field partially or totally compensates the FLT, where such a dependence should be almost absent.

The effect of the FLT on the skyrmion dynamics can be also analytically demonstrated by including into the Thiele equation developed in Refs. [54,60] the DLT due to the SHE. The magnetization distribution of the magnetic Néel skyrmion can be represented in the form $\mathbf{m}(\mathbf{r}, t) = \sin\theta(\rho, t)\hat{\rho} + \cos\theta(\rho, t)\hat{z}$ with $\mathbf{r} = (x, y)$ and taking into account a slow dependence on time [54]. Hence, the generalized Thiele equation reads

$$\mathbf{G} \times \mathbf{v} - \alpha \overleftrightarrow{\mathcal{D}} \cdot \mathbf{v} + 4\pi d'_j \overleftrightarrow{\mathcal{R}}\left(\phi_0 = \frac{\pi}{2}\right) \cdot \mathbf{j_{HM}} + \mathbf{F} = 0. \quad (4)$$

On the first member, $\mathbf{G}$ is the "gyrocoupling vector" with $\mathbf{G} = -4\pi Q\,\hat{z}$; $Q = -1$ is the topological charge; $\mathbf{v} = \dot{\mathbf{R}}(t)$ ("•" denotes the time derivative and $t = \frac{\tau}{\gamma_0 M_s}$ is

TABLE II. Summary of the directions of motion of a skyrmion under the effect of different sources. X indicates which source of motion is active. FLT and DLT are considered for positive field and current.

Breathing mode	FLT	DLT	X direction	Y direction
X			No motion	No motion
	X		No motion	No motion
		X	Negative (small)[a]	Negative
X	**X**		Positive	Negative (small)
X		**X**	Negative (small)[a]	Negative
	X	**X**	Negative (small)[a]	Negative
X	**X**	**X**	Negative/positive depending on DLT and FLT[b]	Negative

[a]See Supplemental Material [43], movie 3.
[b]See Supplemental Material [43], movie 4.

the time) is the drift velocity with $\mathbf{R} = (X, Y)$ the skyrmion guiding center experiencing the effect of the in-plane bias field that coincides with the geometric center for a symmetric skyrmion; $\overleftrightarrow{\mathcal{D}} = \int (\frac{\partial \langle \mathbf{m_0} \rangle}{\partial \tilde{r}_\alpha} \cdot \frac{\partial \langle \mathbf{m_0} \rangle}{\partial \tilde{r}_\beta}) d\tilde{x}\, d\tilde{y}$ is the dissipative tensor ($\langle \dots \rangle$ denotes the time average over a single period T of the microwave excitation) function of the shape of the skyrmion expressed in terms of the scaled components $\tilde{r}_\alpha(\tilde{r}_\beta) \rightarrow \frac{r_\alpha}{L_{sc}}(\frac{r_\beta}{L_{sc}})$ with $\alpha, \beta = x, y$; $d_j{}' = \gamma_0 M_s d_j L_{sc} I$ with $I = \frac{1}{4}\int_0^\infty d\tilde{\rho}(\sin\theta\cos\theta + \tilde{\rho}\frac{d\theta}{d\tilde{\rho}})$ a dimensionless integral in the dimensionless variable $\tilde{\rho}$ (θ is the polar angle); and $\overleftrightarrow{\mathcal{R}}$ is the in-plane rotation matrix depending on the azimuthal angle ϕ_0 [10]. $\mathbf{F}$ is the "force" resulting from the in-plane external field with $F_\alpha = -\gamma_0 L_{sc} \int \langle \mathbf{m_0} \rangle \cdot (\frac{\partial \langle \mathbf{m_0} \rangle}{\partial \tilde{r}_\alpha} \times \langle \mathbf{m} \times \mathbf{H}_{eff} \rangle) d\tilde{x} d\tilde{y}$ with $\alpha = x, y$, where $\langle \mathbf{m} \rangle = \langle \mathbf{m}_0 + \delta\mathbf{m} \rangle$ with $\delta\mathbf{m} \ll \mathbf{m}_0$ the fast time-dependent dynamic part being $\delta\mathbf{m} \ll \mathbf{m}_0$ [54].

From Eq. (4), by following similar calculation as in Ref. [10], we can determine the skyrmion velocity components:

$$\begin{pmatrix} v_x \\ v_y \end{pmatrix} = -d_j' \begin{pmatrix} -\frac{\alpha\mathcal{D}}{1+\alpha_G{}^2\mathcal{D}^2} & \frac{1}{1+\alpha^2\mathcal{D}^2} \\ -\frac{1}{1+\alpha^2\mathcal{D}^2} & -\frac{\alpha\mathcal{D}}{1+\alpha^2\mathcal{D}^2} \end{pmatrix} \begin{pmatrix} j_{HM} \\ 0 \end{pmatrix} - \begin{pmatrix} -\frac{\alpha\mathcal{D}}{1+\alpha^2\mathcal{D}^2} & \frac{1}{1+\alpha^2\mathcal{D}^2} \\ -\frac{1}{1+\alpha^2\mathcal{D}^2} & -\frac{\alpha\mathcal{D}}{1+\alpha^2\mathcal{D}^2} \end{pmatrix} \begin{pmatrix} \tilde{F}_x \\ \tilde{F}_y \end{pmatrix},$$

with $\mathcal{D} \approx 1$ and $\tilde{F}_\alpha = {}^{F_\alpha}/_{4\pi}$ yielding

$$\begin{cases} v_x = d_j' \frac{\alpha\mathcal{D}}{1+\alpha^2\mathcal{D}^2} j_{HM} + \frac{\alpha\mathcal{D}}{1+\alpha^2\mathcal{D}^2}\tilde{F}_x - \frac{1}{1+\alpha^2\mathcal{D}^2}\tilde{F}_y \\ v_y = d_j' \frac{1}{1+\alpha^2\mathcal{D}^2} j_{HM} + \frac{1}{1+\alpha^2\mathcal{D}^2}\tilde{F}_x + \frac{\alpha\mathcal{D}}{1+\alpha^2\mathcal{D}^2}\tilde{F}_y \end{cases}. \quad (5)$$

Then, the skyrmion Hall angle can be computed:

$$\phi_{SH} = \arctan\left[\frac{d_j' j_{HM} + \alpha\mathcal{D}\tilde{F}_y + \tilde{F}_x}{d_j'\alpha\mathcal{D} j_{HM} + \alpha\mathcal{D}\tilde{F}_x - \tilde{F}_y}\right]. \quad (6)$$

We note that, at fixed current density j_{HM}, ϕ_{SH} decreases, for example, when the total force increases negatively.

For $j_{HM} = 0$ and for small damping $\alpha \ll 1$, we get $v_x \simeq -\tilde{F}_y$ and $v_y \simeq 0$ (being $\tilde{F}_x$ small) in agreement with Ref. [54], where $v_x \approx F_y/(4\pi Q)$ with $Q = -1$. In our analytical study, a negative $\tilde{F}_y$ corresponds to a positive applied field and we obtain that if $F_y < 0 (F_y > 0)$ we get $v_x > 0$ ($v_x < 0$). In other words, when the DLT is absent, the FLT promotes a prevalent skyrmion motion along the x direction for an applied field along the y direction. This qualitative discussion on the analytical approach is consistent with the micromagnetic simulations shown in Fig. 6 and with the summary in Table II.

Eventually, to quantitatively compare the micromagnetic simulations with experimental measurements, the following procedure should be applied.

(1) For each value of the applied current j_{HM}, determine experimentally the corresponding FLT and DLT, as done in Ref. [34].

(2) From Eq. (1) $\nu = \frac{\partial FLT}{\partial DLT}$; therefore, from the experimental data of the previous point, it is possible to obtain the real dependence $\nu(j_{HM})$ (it can be either linear or nonlinear; see possible qualitative examples indicated in Fig. 8, where ν can be either positive or negative due to the fact that DLT and FLT can have opposite signs [34]).

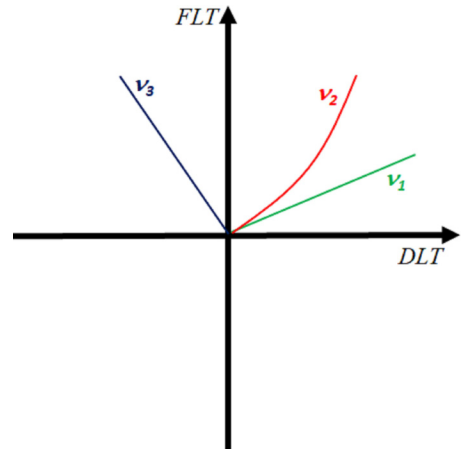

FIG. 8. Qualitative example of the ν dependence on the DLT and FLT.

(3) Perform micromagnetic simulations with the real ν to estimate the skyrmion Hall angle.

In this way, it would be possible to quantitatively determine the skyrmion Hall angle as a function of j_{HM}.

V. SUMMARY AND CONCLUSIONS

In summary, we have performed a numerical experiment based on micromagnetic simulations to understand the effect of SHE-FLT and DLT on a nonrigid (breathing) skyrmion. We have preliminarily demonstrated that the breathing of the skyrmion can be originated by thermal fluctuations. We have also shown that the SHE-FLT and DLT promote two antagonist skyrmion motions: the former occurs mainly along the x axis, while the latter occurs mainly along the y direction. Therefore, the combination of the breathing mode and a sufficiently large SHE-FLT gives rise to the current dependence of the SHA, as observed in the experiments [27,28]. Our result is qualitatively confirmed by a generalized Thiele equation and could be confirmed by an experiment, where the SHA should be characterized as a function of an in-plane field for different currents. According to the amplitude of the range where the SHA exhibits the current dependence, it would be possible to estimate the effect of the SHE-FLT.

ACKNOWLEDGMENTS

This work was supported by the executive programme of scientific and technological cooperation between Italy and China for the years 2016–2018 (2016YFE0104100) entitled "Nanoscale broadband spin-transfer-torque microwave detector" funded by Ministero degli Affari Esteri e della Cooperazione Internazionale (Code No. CN16GR09). R.T. and G.F. also thank the project "ThunderSKY" funded from the Hellenic Foundation for Research and Innovation and the General Secretariat for Research and Technology, under Grant No. 871. R.Z. acknowledges support by Gruppo Nazionale per la Fisica Matematica (GNFM) and Istituto Nazionale di Alta Matematica (INdAM) "F. Severi."

[1] N. Nagaosa and Y. Tokura, Nat. Nanotechnol. **8**, 899 (2013).
[2] A. Soumyanarayanan, N. Reyren, A. Fert, and C. Panagopoulos, Nature (London) **539**, 509 (2016).
[3] G. Finocchio, F. Büttner, R. Tomasello, M. Carpentieri, and M. Kläui, J. Phys. D **49**, 423001 (2016).
[4] I. Dzyaloshinsky, J. Phys. Chem. Solids **4**, 241 (1958).
[5] T. Moriya, Phys. Rev. Lett. **4**, 228 (1960).
[6] S. Muhlbauer, B. Binz, F. Jonietz, C. Pfleiderer, A. Rosch, A. Neubauer, R. Georgii, and P. Boni, Science **323**, 915 (2009).
[7] X. Z. Yu, Y. Onose, N. Kanazawa, J. H. Park, J. H. Han, Y. Matsui, N. Nagaosa, and Y. Tokura, Nature (London) **465**, 901 (2010).
[8] S. X. Huang and C. L. Chien, Phys. Rev. Lett. **108**, 267201 (2012).
[9] J. Sampaio, V. Cros, S. Rohart, A. Thiaville, and A. Fert, Nat. Nanotechnol. **8**, 839 (2013).
[10] R. Tomasello, E. Martinez, R. Zivieri, L. Torres, M. Carpentieri, and G. Finocchio, Sci. Rep. **4**, 6784 (2014).
[11] W. Jiang, P. Upadhyaya, W. Zhang, G. Yu, M. B. Jungfleisch, F. Y. Fradin, J. E. Pearson, Y. Tserkovnyak, K. L. Wang, O. Heinonen, S. G. E. te Velthuis, and A. Hoffmann, Science **349**, 283 (2015).
[12] C. Moreau-Luchaire, C. Moutafis, N. Reyren, J. Sampaio, C. A. F. Vaz, N. Van Horne, K. Bouzehouane, K. Garcia, C. Deranlot, P. Warnicke, P. Wohlhüter, J.-M. George, M. Weigand, J. Raabe, V. Cros, and A. Fert, Nat. Nanotechnol. **11**, 444 (2016).
[13] O. Boulle, J. Vogel, H. Yang, S. Pizzini, D. de S. Chaves, A. Locatelli, T. O. M. A. Sala, L. D. Buda-Prejbeanu, O. Klein, M. Belmeguenai, Y. Roussigné, A. Stashkevich, S. M. Chérif, L. Aballe, M. Foerster, M. Chshiev, S. Auffret, I. M. Miron, and G. Gaudin, Nat. Nanotechnol. **11**, 449 (2016).
[14] S. Woo, K. Litzius, B. Krüger, M.-Y. Im, L. Caretta, K. Richter, M. Mann, A. Krone, R. M. Reeve, M. Weigand, P. Agrawal, I. Lemesh, M.-A. Mawass, P. Fischer, M. Kläui, and G. S. D. Beach, Nat. Mater. **15**, 501 (2016).
[15] A. N. Bogdanov, U. K. Rößler, M. Wolf, and K.-H. Müller, Phys. Rev. B **66**, 214410 (2002).
[16] A. K. Nayak, V. Kumar, T. Ma, P. Werner, E. Pippel, R. Sahoo, F. Damay, U. K. Rößler, C. Felser, and S. S. P. Parkin, Nature (London) **548**, 561 (2017).
[17] M. Hoffmann, B. Zimmermann, G. P. Müller, D. Schürhoff, N. S. Kiselev, C. Melcher, and S. Blügel, Nat. Commun. **8**, 308 (2017).
[18] H.-B. Braun, Adv. Phys. **61**, 1 (2012).
[19] F. Büttner, I. Lemesh, M. Schneider, B. Pfau, C. M. Günther, P. Hessing, J. Geilhufe, L. Caretta, D. Engel, B. Krüger, J. Viefhaus, S. Eisebitt, and G. S. D. Beach, Nat. Nanotechnol. **12**, 1040 (2017).
[20] G. Bourianoff, D. Pinna, M. Sitte, and K. Everschor-Sitte, AIP Adv. **8**, 055602 (2018).
[21] R. Tomasello, K. Y. Guslienko, M. Ricci, A. Giordano, J. Barker, M. Carpentieri, O. Chubykalo-Fesenko, and G. Finocchio, Phys. Rev. B **97**, 060402 (2018).
[22] C. Schutte, J. Iwasaki, A. Rosch, and N. Nagaosa, Phys. Rev. B **90**, 174434 (2014).
[23] J. Iwasaki, M. Mochizuki, and N. Nagaosa, Nat. Nanotechnol. **8**, 742 (2013).
[24] S. Zhang and Z. Li, Phys. Rev. Lett. **93**, 127204 (2004).
[25] J. E. Hirsch, Phys. Rev. Lett. **83**, 1834 (1999).
[26] J. Sinova, S. O. Valenzuela, J. Wunderlich, C. H. Back, and T. Jungwirth, Rev. Mod. Phys. **87**, 1213 (2015).
[27] W. Jiang, X. Zhang, G. Yu, W. Zhang, X. Wang, M. Benjamin Jungfleisch, J. E. Pearson, X. Cheng, O. Heinonen, K. L. Wang, Y. Zhou, A. Hoffmann, and S. G. E. te Velthuis, Nat. Phys. **13**, 162 (2016).
[28] K. Litzius, I. Lemesh, B. Krüger, P. Bassirian, L. Caretta, K. Richter, F. Büttner, K. Sato, O. A. Tretiakov, J. Förster, R. M. Reeve, M. Weigand, I. Bykova, H. Stoll, G. Schütz, G. S. D. Beach, and M. Kläui, Nat. Phys. **13**, 170 (2016).
[29] G. Yu, P. Upadhyaya, X. Li, W. Li, S. K. Kim, Y. Fan, K. L. Wong, Y. Tserkovnyak, P. K. Amiri, and K. L. Wang, Nano Lett. **16**, 1981 (2016).
[30] S. Woo, K. M. Song, X. Zhang, Y. Zhou, M. Ezawa, X. Liu, S. Finizio, J. Raabe, N. J. Lee, S.-I. Kim, S.-Y. Park, Y. Kim, J.-Y. Kim, D. Lee, O. Lee, J. W. Choi, B.-C. Min, H. C. Koo, and J. Chang, Nat. Commun. **9**, 959 (2018).
[31] X. Zhang, Y. Zhou, and M. Ezawa, Nat. Commun. **7**, 10293 (2016).
[32] R. Tomasello, V. Puliafito, E. Martinez, A. Manchon, M. Ricci, M. Carpentieri, and G. Finocchio, J. Phys. D **50**, 325302 (2017).
[33] J. Barker and O. A. Tretiakov, Phys. Rev. Lett. **116**, 147203 (2016).
[34] M. H. Nguyen, D. C. Ralph, and R. A. Buhrman, Phys. Rev. Lett. **116**, 126601 (2016).
[35] L. Lopez-Diaz, D. Aurelio, L. Torres, E. Martinez, M. a Hernandez-Lopez, J. Gomez, O. Alejos, M. Carpentieri, G. Finocchio, and G. Consolo, J. Phys. D **45**, 323001 (2012).
[36] A. Giordano, G. Finocchio, L. Torres, M. Carpentieri, and B. Azzerboni, J. Appl. Phys. **111**, 07D112 (2012).
[37] W. F. Brown, Phys. Rev. **130**, 1677 (1963).
[38] G. Finocchio, I. N. Krivorotov, X. Cheng, L. Torres, and B. Azzerboni, Phys. Rev. B **83**, 134402 (2011).
[39] J. Zázvorka, F. Jakobs, D. Heinze, N. Keil, S. Kromin, S. Jaiswal, K. Litzius, G. Jakob, P. Virnau, D. Pinna, K. Everschor-Sitte, A. Donges, U. Nowak, and M. Kläui, arXiv:1805.05924 (2018).
[40] N. E. Huang, Z. Shen, S. R. Long, M. C. Wu, H. H. Shih, Q. Zheng, N.-C. Yen, C. C. Tung, and H. H. Liu, Proc. R. Soc. A **454**, 903 (1998).
[41] N. E. Huang, Z. Shen, and S. R. Long, Annu. Rev. Fluid Mech. **31**, 417 (1999).
[42] P. Flandrin, G. Rilling, and P. Goncalves, IEEE Signal Process. Lett. **11**, 112 (2004).
[43] See Supplemental Material at http://link.aps.org/supplemental/10.1103/PhysRevB.98.224418 for the details of HHT and wavelet transforms, for the micromagnetic framework to calculate the FMR response of the skyrmion, as well as for the four movies.
[44] S. Mallat, *A Wavelet Tour of Signal Processing* (Elsevier, New York, 2009).
[45] G. Siracusano, G. Finocchio, A. La Corte, G. Consolo, L. Torres, and B. Azzerboni, Phys. Rev. B **79**, 104438 (2009).
[46] Z. K. Peng, P. W. Tse, and F. L. Chu, Mech. Syst. Signal Process. **19**, 974 (2005).
[47] A. Ayenu-Prah and N. Attoh-Okine, Adv. Adapt. Data Anal. **02**, 1 (2010).
[48] A. Komaty, A. Boudraa, and D. Dare, in *2012 IEEE International Symposium on Signal Processing Information Technology*

(ISSPIT), 12-15 Dec. 2012, Ho Chi Minh City, Vietnam (IEEE, Piscataway, NJ, 2012), pp. 292–297.

[49] G. Siracusano, A. La Corte, V. Puliafito, and G. Finocchio, J. Appl. Phys. **115**, 17D108 (2014).

[50] G. Siracusano, F. Lamonaca, R. Tomasello, F. Garescì, A. La Corte, D. L. Carnì, M. Carpentieri, D. Grimaldi, and G. Finocchio, Mech. Syst. Signal Process. **75**, 109 (2016).

[51] G. Finocchio, G. Siracusano, V. Tiberkevich, I. N. Krivorotov, L. Torres, and B. Azzerboni, Phys. Rev. B **81**, 184411 (2010).

[52] L. Rózsa, U. Atxitia, and U. Nowak, Phys. Rev. B **96**, 094436 (2017).

[53] J.-V. Kim and M.-W. Yoo, Appl. Phys. Lett. **110**, 132404 (2017).

[54] W. Wang, M. Beg, B. Zhang, W. Kuch, and H. Fangohr, Phys. Rev. B **92**, 020403 (2015).

[55] G. Finocchio, M. Ricci, R. Tomasello, A. Giordano, M. Lanuzza, V. Puliafito, P. Burrascano, B. Azzerboni, and M. Carpentieri, Appl. Phys. Lett. **107**, 262401 (2015).

[56] J. C. Slonczewski, Phys. Rev. B **71**, 024411 (2005).

[57] J. C. Slonczewski and J. Z. Sun, J. Magn. Magn. Mater. **310**, 169 (2007).

[58] J.-V. Kim, F. Garcia-Sanchez, J. Sampaio, C. Moreau-Luchaire, V. Cros, and A. Fert, Phys. Rev. B **90**, 064410 (2014).

[59] S.-Z. Lin and A. Saxena, Phys. Rev. B **92**, 180401 (2015).

[60] H. Y. Yuan, X. S. Wang, M. Yung, and X. R. Wang, arXiv:1804.07202 (2018).